Chapter

Application of CFD to Prediction of Heat Exchanger Temperature and Indoor Airflow Control Simulation in Room Air Conditioner Development

Hajime Ikeda, Akinori Sakabe, Shingo Hamada, Mitsuhiro Shirota and Takashi Kobayashi

Abstract

In the development of room air conditioners, repeated experiments are conducted to improve product performance. In experiments, temperatures, and air velocities, however, the number and locations of sensors that can be installed in experiments are limited, and it is difficult to estimate the background of a phenomenon based on experimental data alone. Therefore, in design practice, we utilize quantitative verification by CFD in addition to experimental analysis. In this chapter, we describe two CFD models. The first model is a heat exchanger model of an indoor unit that has a cross-flow fan and a heat exchanger. This model is coupled with CFD model and one-dimensional refrigerant flow circuit model. This calculates airflow velocity, temperature, refrigerant flow pressure, and enthalpy. The second model is an indoor airflow model of a room. The room air conditioner can control the temperature and the velocity distribution of airflow in a room, which influences user thermal comfort by controlling the direction, temperature, and volume of airflow by using the indoor unit outlet. This model can predict airflow velocity and temperature in a room.

Keywords: HVAC, room air conditioner, heat exchanger, refrigeration circuit, indoor airflow

1. Introduction

Wall-mounted room air conditioners were invented in Japan and spread mainly as standard household air conditioners in East Asia. These are split-type air conditioners where the indoor and outdoor units are separate. The indoor unit uses a cross-flow fan, which reduces the depth and length of the unit and allows it to be mounted on a wall. The ability to install the air conditioner on the wall has the advantage of reducing the floor space required for installation. Design problems in indoor units are (1) the

fin-and-tube heat exchanger design and (2) the airflow control. In the following sections, we introduce two numerical models for development of indoor units.

1.1 Fin-and-tube heat exchanger model

Figure 1a is a photo of an indoor unit **Figure 1b** illustrates a sectional view of the internal structure of the indoor unit. The indoor unit consists of three parts: the fin-and-tubes heat exchanger, the cross-flow fan, and the vanes. The internal airflow field pattern can be explained with a two-dimensional sectional view [1, 2]. The fan supplies air for the heat exchanger from the air inlet, the heat exchanger raises the air temperature, and then the vanes control the airflow direction, which enhance the air conditioner's thermal comfort and energy-saving performance.

The fin-and-tube heat exchanger consists of refrigerant tubes inserted into fins. Each tube can be connected with a U-shaped bent tube to form a refrigerant flow circuit with an inlet and outlet for the refrigerant flow (**Figure 1c**). A refrigerant flow circuit has a refrigerant inlet and outlet, and the single continuous tube connecting each is called the "path."

An important improvement for heat exchanger performance is to investigate the air and refrigerant flow in the heat exchanger, identify areas that are causing energy losses that do not contribute to heat exchange between the air and refrigerant flow, and improve those areas.

A main objective of the fin-and-tube heat exchanger model development is to quantify the refrigerant flow state such as pressure, enthalpy, and temperature in wall-mounted indoor unit heat exchangers, especially those units equipped with cross-flow fans.

In previous research papers [3, 4], the heat exchanger was modeled as a straightforward shape (**Figure 2a**). The velocity and direction of the airflow in the heat exchanger were assumed to be unchanged, so that the airflow volume distribution was given in the first row of the tube array and the second and third rows were simply the same as the distribution in the first row. These assumptions allow us to solve for enthalpy of refrigerant flow, pressure, mass flow rate, and heat transfer between the refrigerant flow and air, even when the heat exchanger has multiple paths connected by a distributor device. The previous study [5, 6] developed indoor unit CFD models, which can predict fin pressure loss and heat transfer of fins. These models do not include refrigerant flow calculation, therefore, the transition between the pressure and entropy values from the refrigerant pipe inlet to the outlet in the path design was unknown. The previous study [7] developed an inclined heat exchanger CFD model

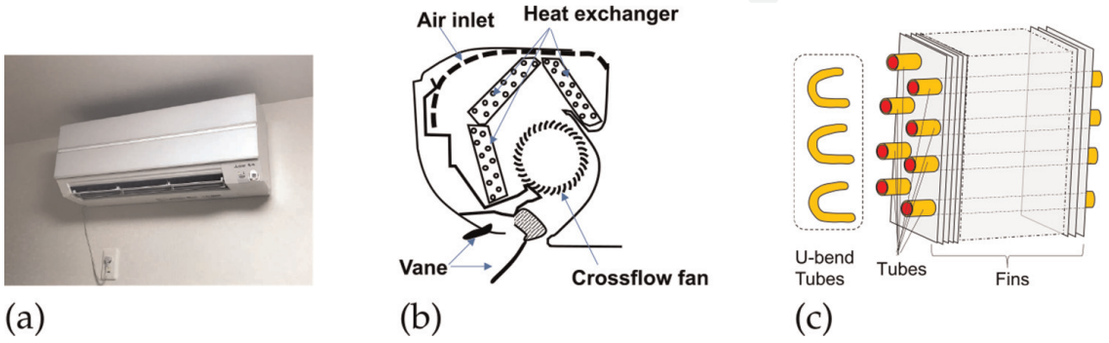

Figure 1.
Indoor unit: (a) a photo of an indoor unit, (b) internal structure of indoor unit, and (c) a structure of heat exchanger.

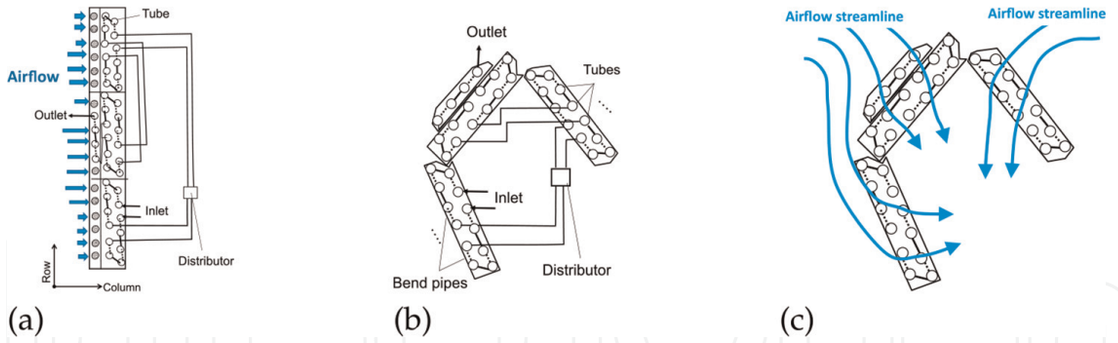

Figure 2.
Heat exchanger modeling: (a) a schematic of previous research model [3, 4], (b) an indoor unit of fin-and-tube heat exchanger, and (c) streamline of indoor unit heat exchanger.

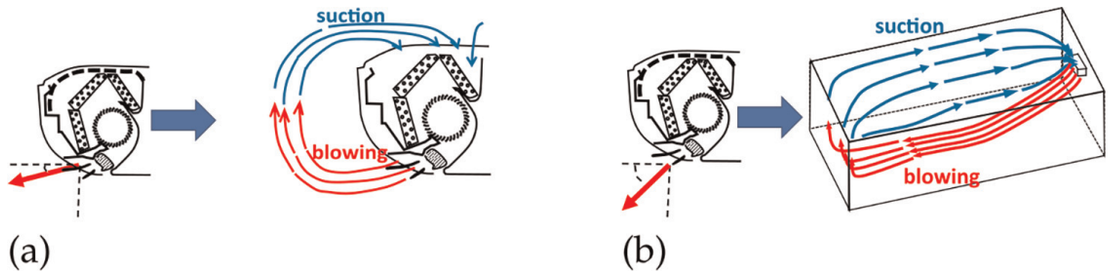

Figure 3.
Indoor airflow control: (a) short airflow circulation and (b) long airflow circulation.

and calculate airflow distribution. It incorporates air flow distribution to refrigerant circuit calculation model, however, this model can reflect indoor unit heat exchanger.

The heat exchanger actually used in the indoor unit is not a straight type but a folded type (**Figure 2b**) and airflow streamline is not a straight but curved form (**Figure 2c**). Since airflow does not flow straight through the first row of tube arrays, it is difficult to determine the air flow rate distribution input to the heat exchanger. Furthermore, the airflow volume distribution in the first row of the tube array is not the same as the tube array in the other rows of the actual heat exchanger, as assumed in previous research papers. Our numerical model is coupled with CFD for air-side calculations and with the one-dimensional refrigerant flow circuit model for refrigerant-side calculations. This CFD model reflects an airflow distribution in the fins and can calculate the pressure and entropy values of the refrigerant flow.

1.2 Indoor airflow model

Figure 3 shows an example of indoor airflow control. A wall-mounted air conditioner was installed on the wall and positioned to blow warm air from a high position in the room. The distance of the blowing air can be varied by controlling the fan speed, heat exchanger temperature, and vane angle. **Figure 3a** is a schematic diagram of short circulation control. The red line represents the airflow moving away from the indoor unit, and the blue line represents the airflow approaching the indoor unit. For explanation, we refer to the red line airflow as the blowing airflow and the blue line airflow as suction airflow. When the vanes are angled upward, the airflow is directed upward. In the heating mode, the temperature of blowing airflow is higher than the air temperature in the room. The blowing airflow floats upward because a buoyant force

works. The airflow circulates near the indoor unit, and the reach of the airflow of the tip is short.

Figure 3b shows a schematic diagram of long circulation control. When the vane is angled down, the airflow is directed downward. Because the suction force is weak, blowing airflow tends to travel farther from the indoor unit and has a long circulatory path.

The airflow control is a technology that sends hot or cold air to various positions. To improve energy-saving performance and comfort, it is optimal to control airflow factors, for example, by avoiding airflow to areas of the room where the user is not present and selectively applying more airflow to body parts that contribute significantly to comfort, such as the feet [8].

If such airflow control can be simulated numerically, the work required for testing the actual equipment can be reduced. The objective of developing indoor airflow model is to replace testing with numerical calculations and to quantitatively evaluate wind velocity and temperature distributions, which are difficult to measure in testing.

Although there have been many studies using CFD in indoor airflow [9], few studies have dealt with split-type air conditioners. Casado et al. [10] verified the airflow temperature distribution using a split-type air conditioner. In this study, the vane angle was fixed. The case where the vane angle and wind direction are varied is verified by Lee S et al. [11]. The numerical model was validated using experimental data under isothermal conditions by varying the vane angle and wind direction. The numerical model was validated using experimental data under non-isothermal conditions with varying vane angles and airflow directions. Experimental data under non-isothermal conditions were used to validate the numerical model. Temperature distributions were obtained when the air conditioner was operated in heating mode and the vane angle and airflow rate were varied.

2. Fin and tube heat exchanger model

2.1 Numerical model

Our numerical model couples with CFD for air-side calculations and with the one-dimensional refrigerant circuit model for refrigerant-side calculations. The air-side model consist of two CFD models. The first model calculates airflow velocity and pressure by solving an unsteady Reynolds-averaged Navier–Stokes (RANS) equation model. The second model calculates airflow temperature and amount of heat exchange of each tube by using first model calculation result. This model solves a steady heat conductivity equation where the airflow velocity field calculation result is fixed. The refrigerant flow side model can calculate refrigerant flow pressure, enthalpy, and flow rates on each tube by using circuit model of a heat exchanger path. This model inputs heat of tubes from the air-side model result. **Table 1** denotes the input and output relationship of these models.

2.1.1 Air-side model

A commercial CFD software, SCRYU/Tetra (CRADLE 2018) [12], was used for air-side models. Two air-side CFD models, airflow model, and heat conductivity model use same CFD mesh. **Figure 4** shows the CFD mesh of the overall heat exchanger and the cross-flow fan, and **Figure 4b** shows the fin surface mesh. This mesh consists of a

Model	Method	Inputs	Outputs
Air-side model	CFD (airflow)	Fan rotate speed	Velocity and pressure
	CFD (heat conductivity)	Temperature of tubes	Heat of tubes
Refrigerant flow-side model	One-dimensional circuit model	heat of tubes	temperature of tubes

Table 1.
Fin-and-tube heat exchanger model.

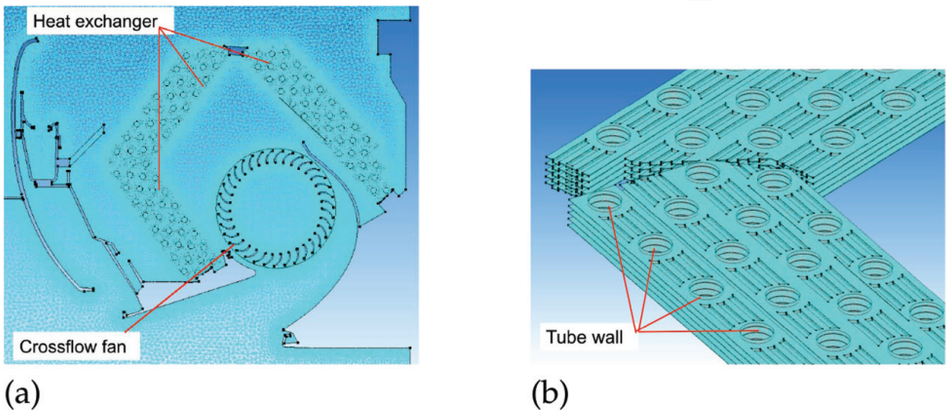

Figure 4.
Mesh of indoor unit: (a) internal of indoor unit and (b) fins and tubes. Tube walls are boundary condition regions of CFD (heat conductivity) model, which can be set to temperature from the result of refrigerant flow-side model.

stationary region mesh and a rotating region mesh. For rotating region, we created 0.25 mm to 0.50 mm tetrahedral meshes. Four prism meshes of 0.1 mm are inserted along the fan surface. Arbitrary Lagrangian Euler (ALE) method is adopted for fan rotating calculation. A tetrahedral unstructured mesh size was 0.25 mm to 50 mm and further prism layers were inserted along the walls. For fin walls, tetrahedral mesh size is 0.25 mm and 0.1 mm; two prism layers were inserted along the walls. Actual typical indoor unit heat exchanger width is 666 mmm and has about 555 fins. In order to limit the number of meshes and perform calculations efficiently within our computational resource, we designed our numerical model to have width of 6.0 mm and five fins. Previous research papers [2, 5] used two dimensional CFD model for simulating cross-flow fan airflow pattern. We used thin CFD model (6.0 mm width model) that models a the cross-sectional view at a representative position. For the thin width, this model airflow pattern is two dimensional. However, the actual indoor unit has filters and unit ribs that block the airflow at some positions. The cross-sectional view of the indoor unit has different shapes in different positions and, therefore, airflow patterns are different at these positions. When calculating the amount of heat exchange for each tube, the results are multiplied by 100.0, which is an adjusted constant to consider the influence of some different shapes of cross-sectional view of the actual unit.

2.1.2 Refrigerant flow-side model

We constructed a circuit model, which is made of node elements and tube elements to solve refrigerant flow state (**Figure 5a**). The node element preserves

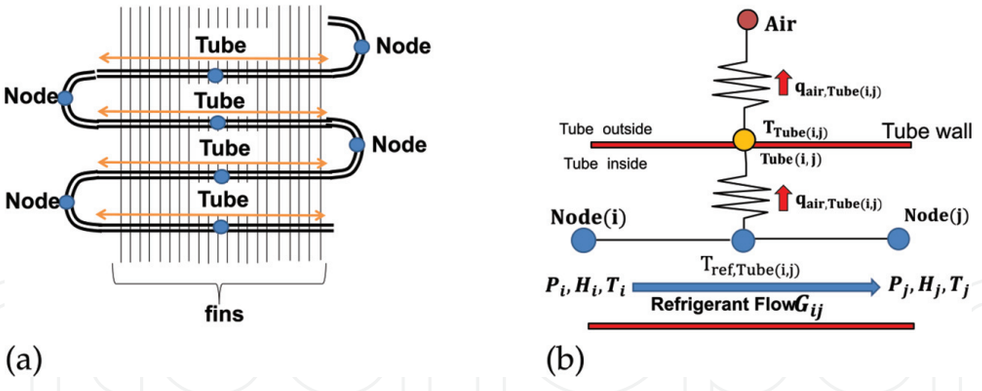

Figure 5.
Refrigerant flow circuit model: (a) arrangement of node and tube elements in the heat exchanger and (b) a relationship of the node and tube elements.

refrigerant flow temperature T (°C), enthalpy H (kJ/kg), and pressure P (Pa). The tube element is connected to two node elements. It preserves the tube length l (m), tube inner diameter ϕ (m), the refrigerant flow rate G (kg/s), the amount of heat transfer between refrigerant flow and the air q_{air} (W), and tube wall temperature T_{tube}. The distributor can be modeled with more than three node elements with tube elements. **Figure 5b** shows the relationship of the node and tube elements, indicated by the two nodes: Node (i) and Node (j), the tube elements connecting with Node (i) and Node (j) represented by Tube (ij).

Let P_i be the element pressure of Node (i), $T_i$be the temperature, and H_i be the enthalpy. The difference of Node (i) pressure P_i and Node (j) pressure P_j can be written by using the function $\Delta P\left(G_{ij}, \phi_{ij}, l_{ij}\right)$, which calculates pressure loss from the Tube (ij) refrigerant flow rate G_{ij} using Blasius equation and Lockhart-Martinelli correlation [3]. The relationship of P_i, P_j, and $\Delta P\left(G_{ij}, \phi_{ij}, l_{ij}\right)$ is as in Eq. (1).

$$P_i - P_j = \Delta P(G, \phi, l) \tag{1}$$

The relationship of the connecting node elements Node (i) and Node (j), enthalpy H_i, H_j, and G_{ij} is shown in Eq. (2).

$$H_i - H_j = q_{air,ij}/G_{i,j} \tag{2}$$

Suppose that the refrigeration circuit reaches the steady state, at any node element Node (j), the total refrigerant flow rate is equal to 0 (kg/s).

$$\sum_{j=1} G_{i,j} = 0 \tag{3}$$

Eq. (1) is the momentum conservation equation, Eq. (2) is the energy conservation equation, and Eq. (3) is the mass conservation equation.

Assuming that the number of node elements is n and the number of tube elements is m, the number of unknown variables is n each for P_i and H_i, and m for G_{ij}, for a total unknown variable is $2n + m$. The number of equations is n for each of Eqs. (2) and (3), and m for Eq. (3), for a total number of equations is $2n + m$. Since the number of unknown variables and the number of equations are equal, the value of the unknown

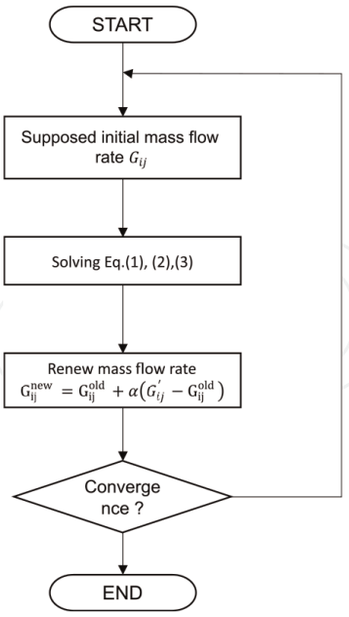

Figure 6.
Flowchart of refrigerant flow circuit model.

variable can be uniquely determined from equations Eq. (1), (2), and (3). **Figure 6** is a heat exchanger calculation flowchart. We can obtain refrigerant flow P_i (Pa) and enthalpy H_i kJ/kg for all node elements.

We can calculate temperature of node elements T_i from P_i and H_i by using refrigerant property database REFPROP [13]. We introduce the refrigerant flow temperature of $Tube_{ij}$ element as $T_{ref} = (T_i + T_j)/2$ (°C). We can then calculate wall temperature $T_{tube,ij}$ from the heat transfer rate of tube α_{ij} (W/m^{2}K), tube surface S_{ij} (m^2), tube wall thickness t (m), and tube wall heat conductivity (W/m^{2}K) as follows:

$$T_{tube,ij} = T_{ref} + \left(\frac{1}{\alpha_{ij} s_{ij}} + \frac{t}{\lambda}\right)^{-1} q_{air,ij} \tag{4}$$

2.1.3 Coupling calculation

Figure 7 is a flowchart of coupling calculation. Initially, the air-side CFD (airflow) is performed once. Then each tube wall temperature $T_{tube,ij}$is assumed as the initial condition and CFD (heat conductivity) process is performed. This CFD (heat conductivity) process outputs each tube $q_{air,ij}$. Third, the refrigeration circuit simulation process calculates the refrigerant flow state using $q_{air,ij}$ and outputs$T_{tube,ij}$, which are different from the CFD initial condition $T_{tube,ij}$. The second and third process is an iterative loop processes.

In the previous research [5], it was necessary to fix the temperature of the tubes $T_{tube,ij}$i to perform the CFD (heat conductivity). In addition, it was not possible to calculate refrigerant enthalpy. In this coupled calculation, the heat transfer from the air to the refrigerant flow is the same value ($q_{air,ij}$) for both the air-side and refrigerant flow calculations. This makes it possible to calculate the refrigerant enthalpy at the same time the temperature of tubes is calculated iteratively.

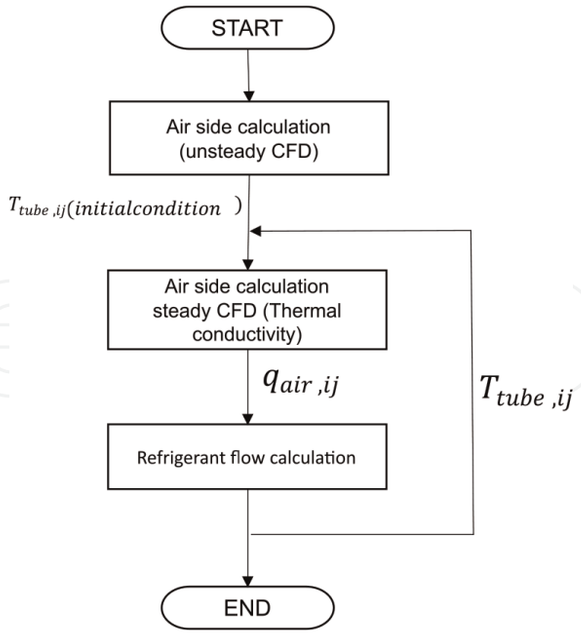

Figure 7.
Flowchart of coupled simulation.

	Fan rotation speed (rpm)	Volume rate (m^3/min)	Capacity (W)
Experimental	1555 (1.00)	22.2 (1.00)	8000 (1.00)
Numerical model	1550 (0.997)	21.6 (1.03)	8033 (1.04)

Table 2.
Air-side CFD result.

2.2 Result

The coupled calculations were verified using measured data from an actual room air conditioner in heating operation. The heat exchanger has six paths upstream of the refrigerant circuit, four paths in the midstream using a distributor, and two paths further downstream.

Table 2 is comparison of experimental and numerical data of air-side CFD model. Air flow volume rate is from the air-side CFD (airflow) result and heat capacity value is from the air-side CFD (heat conductivity). Amount of heat capacity of CFD is 4% larger than experimental.

Figure 8a and **b** show the air-side CFD (heat conductivity) result at the third run. **Figure 8a** is the airflow velocity contour plot, and **Figure 8b** is the airflow temperature contour plot. The value of the airflow velocity entering the heat exchanger is between 3.0 (m/s) and 4.0 (m/s) at the most area. There are areas where the airflow velocity is lower than 1.0 (m/s), such as at the front bended area and at the part of back of the heat exchanger. Previous research papers [3, 4] assume that the direction of airflow enters vertically into the front of the heat exchanger and direction are not changed, but calculation result shows airflow enter the front of the heat exchanger at various angles and that the direction changes inside the fins.

The air temperature distribution can be roughly classified into three areas. The area with a temperature near 20 °C is the airflow flowing into the inlet of the indoor unit.

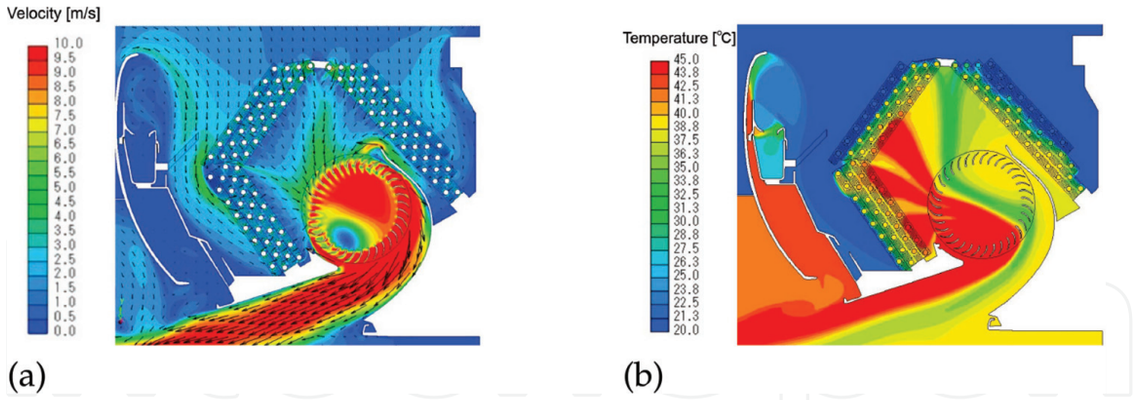

Figure 8.
Result of air-side CFD calculation: (a) airflow velocity contour plot; (b) airflow temperature contour plot.

Since the temperature of the refrigerant state is 20 °C in the liquid phase, the temperature of the airflow passing through the tubes at the top of the heat exchanger, which is in the liquid phase, is around 20 °C. The temperature of the refrigerant state in the two-phase flow is approximately 40 °C. The temperature of the airflow passing through the tubes in the two-phase flow section rises as it exchanges heat with the refrigerant. The tubes of the downwind side of the heat exchanger flow refrigerant vapor phase state, and the temperature of the pipes in the vapor phase exceeds 45 °C. The temperature of the airflow passing through these tubes is above 45 °C.

Figure 9 shows the fin surface temperature, focusing on the part of the fin where conductivity occurs between the vapor phase flow tubes (high temperature) and vapor/liquid phase tube (low temperature). A role of a heat exchanger is a heat exchange function between air and refrigerant. If the temperature difference in the refrigerant piping is large, heat exchange occurs between the refrigerant tubes. In this case, some tubes do not contribute to improved heat capacity, which is called "fin conductivity [4]." These models use fine fin mesh and can calculate heat transfer *via* fins.

Figure 10 shows the result of the refrigeration circuit model calculation using pressure and enthalpy plotted for node elements (p-h diagram). The refrigeration circuit consists of 12 paths. There are two refrigerant inlets, a distributor device, and four outlets. In the heating mode, the enthalpy of refrigerant flow decreases from the refrigerant flow inlet to the outlet because of heat transfer between the refrigerant and

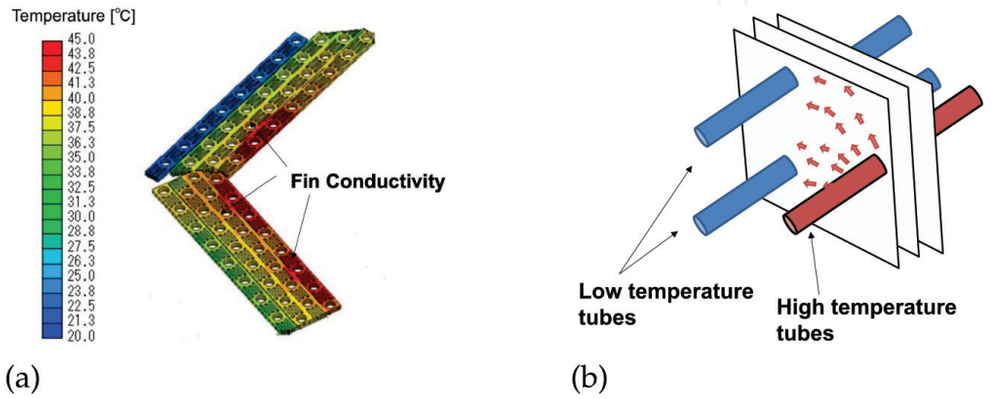

Figure 9.
Fin conductivity: (a) CFD result of fin surface temperature and (b) schematic illustration.

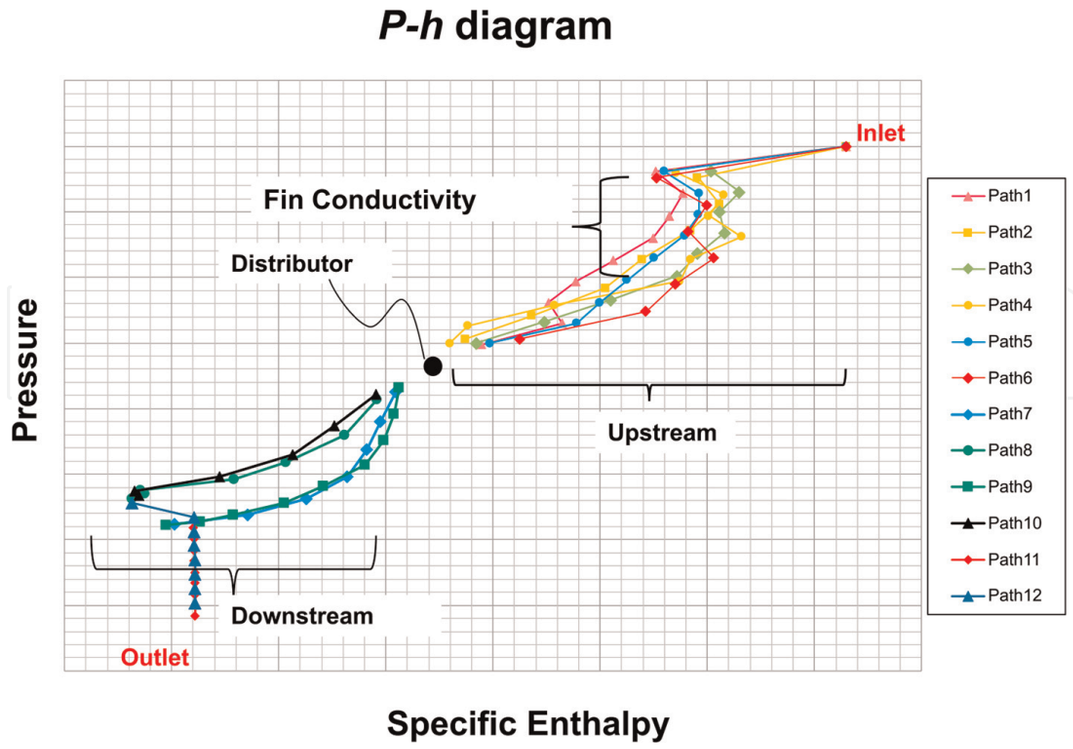

Figure 10.
A p-h diagram of refrigerant flow in the heat exchanger for each of 12 paths. Dots represent pressure and enthalpy values of node elements of tubes. Each path consists of 6 to 8 tubes. The distributor divides these paths into upstream side and downstream side. Paths 1 through 6 are upstream paths, and paths 11 through 12 are downstream paths.

the airflow. This result shows that our numerical model can quantify the energy loss due to fin conductivity.

3. Indoor airflow

3.1 Airflow temperature measurement test room

An airflow temperature measurement test room was used to develop the indoor airflow control model. This test room is constructed with wooden walls, windows, and doors that mimic a room in a Japanese wooden house. The outside air temperature in this room can be controlled by an air conditioning system. This room is equipped with thermocouples, which can measure indoor airflow temperature distribution. **Figure 11** shows the layout of this room and the arrangement of the thermocouples. The air temperature was acquired using a test room with thermocouples taken down from the ceiling. As shown on the right of **Figure 11**, the temperature distribution of the airflow can be visualized by interpolating the temperature in the space without thermocouples through heat conduction calculations.

3.2 Numerical model

3.2.1 Model development

Figure 12 shows how the mesh of the computational model is created. We simplified indoor unit cross-flow fans and vanes to an inlet boundary condition and indoor

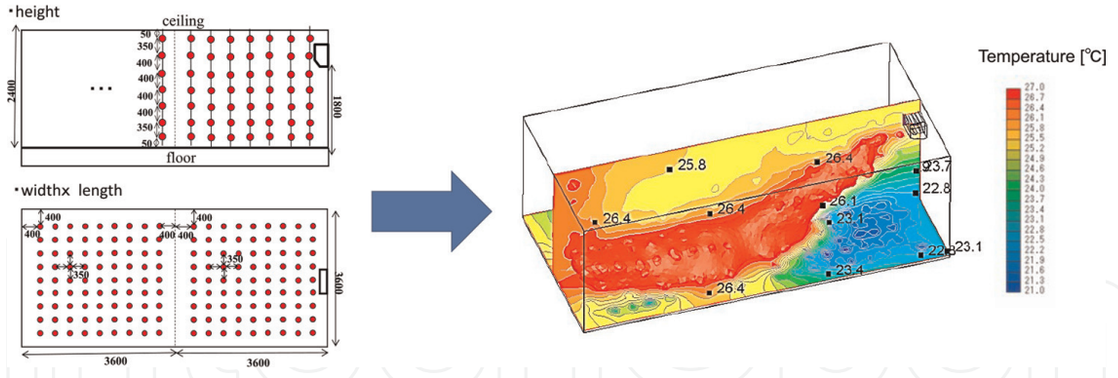

Figure 11.
Schematic diagram of the thermocouple arrangement. The test room is 3.6 (m) deep by 7.2 (m) high by 2.4 (m) wide. Thermocouples are suspended from the ceiling of the test chamber, and thermocouples are placed at intervals of 0.05 to 0.4 (m). A total of 1134 thermocouples were installed in a layout of nine thermocouples in the x direction, 18 in the y direction, and seven pointing in the z direction (height).

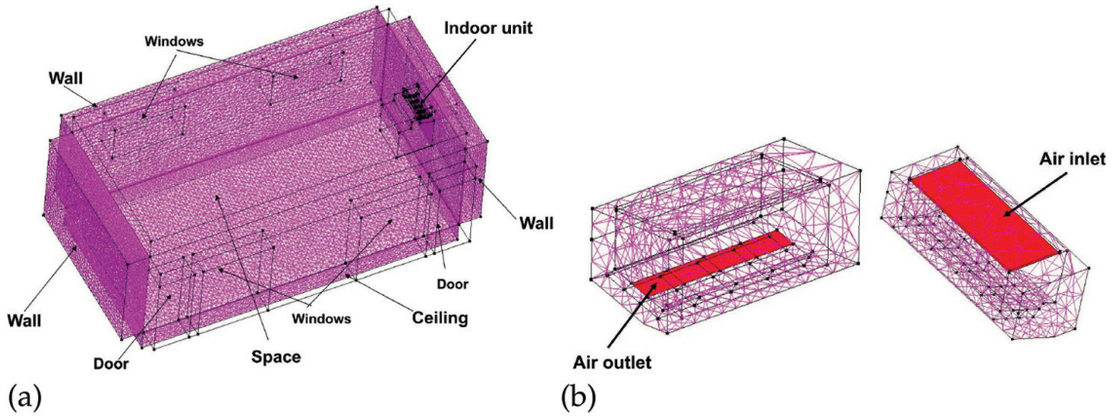

Figure 12.
CFD mesh. This mesh consists of a room space, walls, windows, and a door. The room space is the indoor airflow environment, and wall indicates the floor, ceiling, and front, back, left side, and right side walls. The room air conditioner was installed on a back side wall. Outer surfaces of walls can set outside temperature as the boundary condition.

unit inlet to outlet boundary condition. The boundary conditions for the inlet surface are (1) airflow volume rate, (2) airflow angle, and (3) airflow temperature. The walls, windows, and doors of the test room have small gaps through which drafts can enter and heat can leak out. It is difficult to model heat leakage from a draft numerically because air gap locations are unknown. Therefore, the initial temperature of the wall was set lower than the room temperature to model the heat leakage by the air gaps. The outer surface of the walls was set to the boundary condition of the outside air temperature in the experiment.

3.2.2 Buoyant modeling

We use unsteady RANS model for indoor airflow control model. The governing equations were discretized by the finite volume method and solved using the SIMPLEC method. We used commercial CFD Code SCRYU/Tetra [12] for the calculation. To realize a rotating fan turbulence flow, the inlet condition was also given turbulence kinetic energy of 10 (m^2/s^2) and turbulence dissipation of turbulent kinetic energy of 0.1 (m^2/s^2). These values were obtained from the result of previous air-side

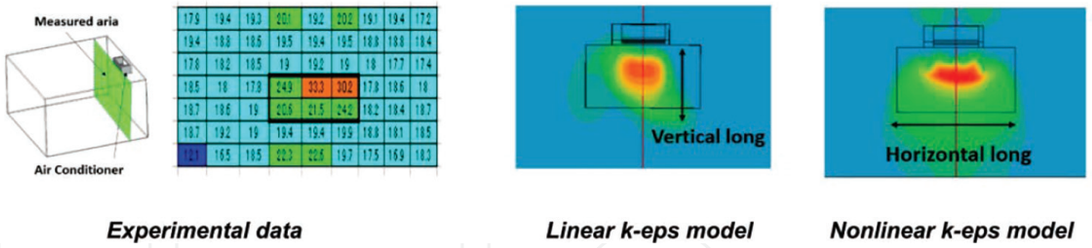

Figure 13.
Temperature distribution. We measured 54 points of air temperature at 0.4 (m) in front of the air conditioner and compared two RANS models.

CFD calculations. The blowing airflow from air outlet is acted as buoyant force, so that the Boussinesq approximation was used for buoyancy force as a momentum conservation equation.

To evaluate the influence of the turbulence model difference, we performed an experiment and two RANS model calculations. One model is linear RANS (standard k-epsilon model) and the other is used nonlinear RANS [14]. **Figure 13** shows the results of an experiment and two calculations. The experimental result and calculation of the nonlinear turbulence model for temperature distribution show the long warm air region in a horizontal direction. Otherwise, linear turbulence model shows a vertical long hot air region. The standard k-epsilon model is isotropic turbulence and the Reynolds stresses act equally in all three directions in three-dimensional space. Since buoyancy forces act only in the vertical direction, they cannot be reproduced by an isotropic model. Therefore, we consider that the anisotropic model is closer to the experimental temperature distribution than the isotropic model. We selected a nonlinear turbulence model for investigating the influence of the buoyancy force.

Table 3 is specification of CFD for our indoor air-control model.

Items	Contents
Turbulence model	Nonlinear RANS [14]
Buoyancy model	Boussinesq approximation
Scheme	SIMPLEC method
Time step	The time step is variable and the coolant number is fixed at 3.0.
Inlet condition	(1) Airflow volume rate, (2) airflow angle, and (3) airflow temperature are set for air-outlet region.
Outlet condition	Same value of airflow volume rate of inlet condition for the air inlet region.

Table 3.
Specification of CFD.

3.3 Experiment

We performed three experiments and calculations using the same control parameter conditions. **Table 4** lists the airflow control parameters of (1) angle (°), (2)

Items	Test (A)	Test (B)	Test (C)
Vane angle (°)	50	50	70
Volume rate (m^3/min	10.7	14.2	12.3
Temperature (°C)	47.2	42.0	45.5

Table 4.
Specification of CFD. Boundary condition for air outlet.

volume rate (m^3/min), and (3) temperature (°C). Angle is defined as the measurement between the horizontal line and the airflow direction.

3.4 Result

In the experiment of **Table 4**, tests (A) and (B) resulted in short airflow circulation. Test (C) resulted in long airflow circulation. We compared the tip of blowing airflow to verify the numerical results.

3.4.1 Short airflow circulation control

Figure 14 compares the airflow tips of tests (A) and (B) with the temperature contour plots at the center of the room. The calculated results are 180 seconds after the initial condition for both (A) and (B). The initial temperature of the indoor air was set to 24 °C and the initial temperature of the wall was 24 °C. Under the conditions of test (A), the blowing airflow floated in the center of the room and did not reach the floor in both experiments and values. However, the distance traveled by the tip of the blowing airflow was different (experimental, 3.6 m; numerical, 2.0 m). Under test (B) conditions, both experimental and numerical airflows contacted the floor; moreover, the distance of the tip of both experimental and numerical airflows was 3.6 (m).

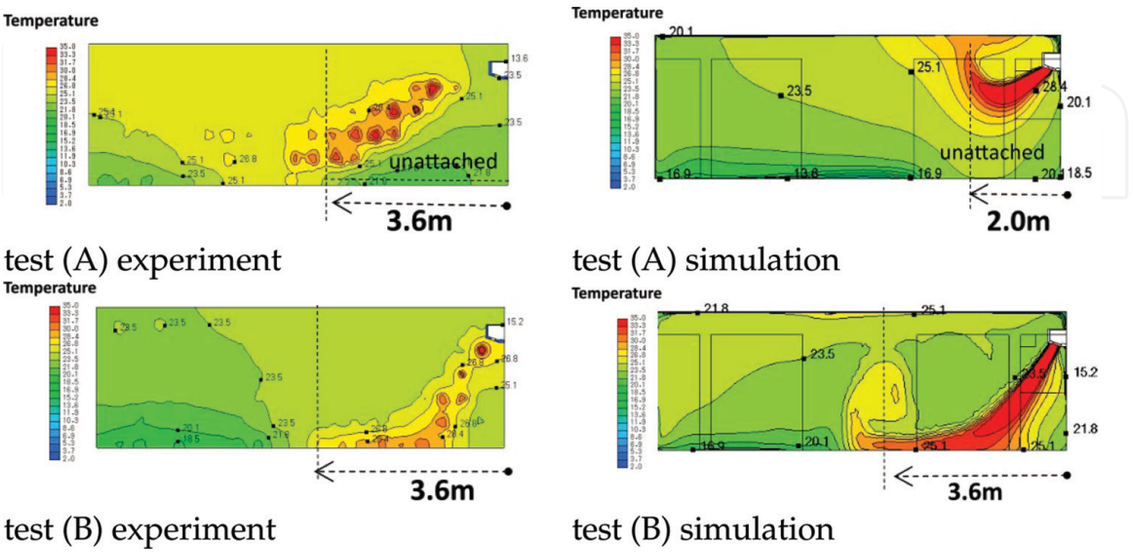

Figure 14.
Indoor airflow experiment and calculation. Comparison of test (A): Both experimental and numerical blowing warm airflow floated in the middle of the room, but the distance traveled by the tip of warm airflow was different. Comparison of test (B): Both experimental and numerical airflow touched the floor.

3.4.2 Long airflow circulation control

Figure 15 shows the results with test (C) conditions. **Figure 15a** visualized measured temperature by experimental thermocouples position. **Figure 15b** is the numerical simulation result of test (C) condition. The initial temperature of the room air was 20 °C, and the initial temperature of the walls was 10 °C. The contour plot is 180 seconds after the initial condition. Under the test (C) conditions, the both experimental and numerical results were such that the blowing airflow reached the floor and the tip of the blowing airflow reached the wall opposite where the room air conditioner was installed.

Figure 16 is three-dimensional isosurface of temperature at 26 °C. In the experiment, the temperature isosurface of 26 °C is limited to the floor, but in the calculation, it reaches the opposite side of the wall where the air conditioner is installed and the isosurface of 26 °C covers the half of the ceiling. In this model, the amount of heat leakage is simulated by using the initial temperature of the room walls as a parameter. This method can adjust the heat balance between the room air and the room walls, but it cannot simulate the airflow from air gaps. In test (C), blowing airflow travels along walls, such as floor and ceiling surfaces. The area where airflow flows along the wall surface in test (C) is larger than that of tests (A) and (B). It is possible that the airflow gaps on the wall surfaces in the test (C) are larger than in tests (A) and (B).

The positions of the arrival of the blowing airflow could be predicted by the calculation model, but the absolute values of the temperature distribution differed between the calculations and experiments.

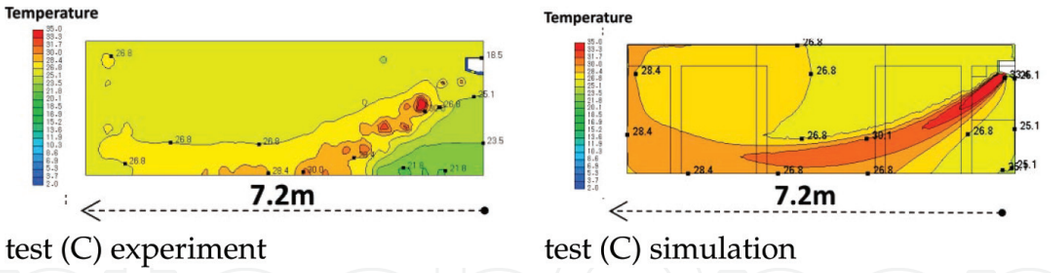

Figure 15.
Indoor airflow experiment. Comparison of test (A): Both experimental and numerical blowing warm airflow reached the back wall of the room.

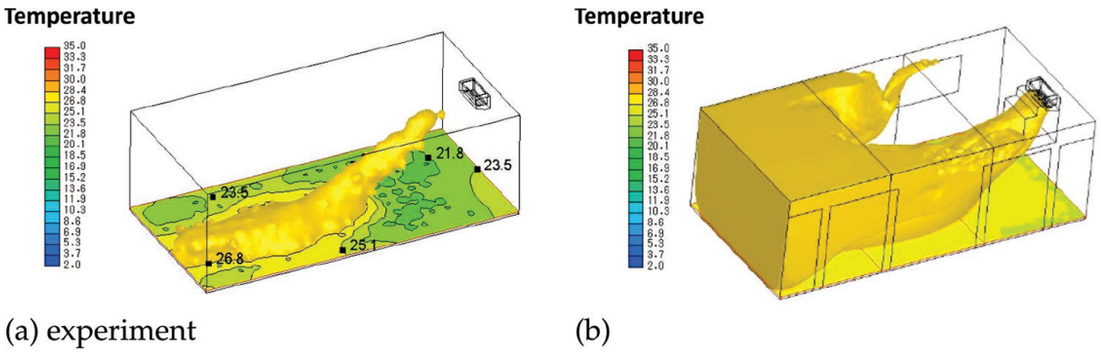

Figure 16.
Indoor airflow experiment and calculation of test (C). The temperature of isosurface is plotted at 26 °C.

When calculations are used as a surrogate model for experiments, it is necessary to analyze the calculation results, taking into account the differences in absolute values of temperature.

We found some differences in the experiments and calculations; however, qualitatively, the airflow calculations are similar to the experiments. The ability to compare experiments and calculations has enabled us to know the difference between experimental and calculated results. By knowing the difference, the number of experiments can be reduced by calculation, thereby reducing the cost of designing airflow control.

4. Conclusions

We described two numerical models for (1) a heat exchanger design and (2) an indoor airflow control. The fin-and-tube heat exchanger model consists of CFD and a one-dimensional refrigerant circuit model. CFD model simulates airflow velocity and temperature, and refrigerant circuit model calculates refrigerant flow pressure and enthalpy. These two models are coupled using the value of amount of heat transfer between air and refrigerant. The indoor airflow model can simulate indoor airflow temperature and velocity by the room air conditioner airflow control. We verified three simulations and the measured temperature data. The arrival position of the blowing air was found to be consistent between experiments and calculations, but some differences were found in the airflow temperature distribution in the room due to the existence of gaps in the wall.

Author details

Hajime Ikeda[1*], Akinori Sakabe[2], Shingo Hamada[2], Mitsuhiro Shirota[2] and Takashi Kobayashi[1]

1 Design System Engineering Center, Mitsubishi Electric Corporation, Tokyo, Japan

2 Shizuoka Works, Mitsubishi Electric Corporation, Tokyo, Japan

*Address all correspondence to: ikeda.hajime@da.mitsubishielectric.co.jp

References

[1] Kohya T. Historical Development of air conditioner technology (in Japanese). 2022. Available from: https://sts.kahaku.go.jp/diversity/document/system/pdf/099.pdf [Accessed 03 November, 2022]

[2] Toffolo A. On the theoretical link between design parameters and performance in cross-flow fans: A numerical and experimental study. Computers & Fluids. 2005;**34**(1):49-66

[3] Jiang H, Aute V, Radermacher R. CoilDesigner: A general-purpose simulation and design tool for air-to-refrigerant heat exchangers. International Journal of Refrigeration. 2006;**29**(4):601-610

[4] Kaga K, Kotoh S, Ogushi T. Prediction of heat exchanger capacity by thermal network method (influence of thermal conduction in fins on capacity of a condenser). Heat Transaction Asian Research. 2008;**37**(2):101-114

[5] Kudoh M, Sasaki S, Hatada T, Morimoto M. A simple method for predicting the performance of a heat exchanger mounted in an air conditioner (1st report, proposed reduced-mesh analysis modeling method). Heat Transaction Asian Research. 2004;**33**(1):12-23

[6] Liu N, Lai XL, Yan K, Zhang H. Investigation of flow and heat transfer characteristics on different heat exchangers of air conditioner. Applied Thermal Engineering. 2016;**103**:428-433

[7] Lee MS, Li Z, Ling J, Aute V. A CFD assisted segmented control volume based heat exchanger model for simulation of air-to-refrigerant heat exchanger with air flow mal-distribution. Applied Thermal Engineering. 2018;**131**:230-243

[8] Huizenga C, Zhang H, Arens E, Wang D. Skin and core temperature response to partial- and whole-body heating and cooling. Journal of Thermal Biology. 2004;**29**(7-8):549-558

[9] Nielsen PV. Fifty years of CFD for room air distribution. Building and Environment. 2015;**91**:78-90

[10] Casado AR, Hajdukiewicz M, de la Flor FS, Jara ER. Calibration methodology for CFD models of rooms and buildings with mechanical ventilation from experimental results. In: Ji G, Zhu J, editors. Computational Fluid Dynamics Simulations [Internet]. London: IntechOpen; 2020 [cited 2022 Nov 06]. Available from: https://www.intechopen.com/chapters/71460. DOI: 10.5772/intechopen.89848

[11] Lee S, Lee J, Kato S. Influence of vane angle on the effectiveness of air conditioning of wall-mounted split-type air conditioners in residential buildings. Science and Technology for the Built Environment. 2017;**23**(5):761-775

[12] Software Cradle Co., Ltd., "SCRYU/Tetra Users Guide"

[13] Huber ML, Lemmon EW, Bell IH, McLinden MO. The NIST REFPROP database for highly accurate properties of industrially important fluids. Industrial and Engineering Chemistry Research. 2022;**61**(42):15449-15472

[14] Batten P, Goldberg U, Chakravarthy S. LNS - An approach towards embedded LES. In: 40th AIAA Aerospace Sciences Meeting & Exhibit. American Institute of Aeronautics and Astronautics